Gain Enhancement of a Dual-Band S-Patch Antenna Array for 5G Application

Dhanapon Udomratanasiri[1], Supakit Kawdungta[1,*], Rassamitut Pansomboon[2], Alongkorn Lang[3] and Chuwong Phongcharoenpanich[3]
[1] Electrical Engineering Department, Faculty of Engineering, Rajamangala University of Technology Lanna, Chang Phueak, Muang, Chiang Mai, 50300, Thailand
[2] National Electronics and Computer Technology Center, National Science and Technology Development Agency, Khlong Nueng, Khlong Luang, Pathum Thani, 12120, Thailand
[3] Telecommunications Engineering Department, School of Engineering, King Mongkut's Institute of Technology Ladkrabang, Lat Krabang, Lat Krabang, Bangkok, 10520, Thailand
***Corresponding Author E-mail:** supakitting@rmutl.ac.th
Received: Feb 17, 2025; **Revised:** Apr 13, 2025; **Accepted:** Apr 22, 2025

Abstract

This paper proposes the dual-band S-patch antenna with gain enhancement by using the planar array configuration and dielectric superstrate. The design of the proposed antenna is focused on the base station antenna in the 5G frequency bands n41 (2.6 GHz) and n78 (3.5 GHz). The dual-band S-patch antenna is arranged in the 2 × 6 elements planar array antenna and the FR4 dielectric superstrate is on the top of the array. The simulated results indicated that the operating frequency of 2.55–2.65 GHz and 3.46–3.61 GHz with uni-directional radiation pattern. The antenna gain can be improved with 18.70 dBi at 2.6 GHz and 19.30 dBi at 3.5 GHz. The prototype antenna is fabricated and the measured results are in good agreement. With the simple design of the proposed antenna, it would be useful for the installation of the base station antenna.

Keywords: Antenna Array, Dual-Band, S-Patch, Superstrate

1. Introduction

One of the growing wireless communication technologies is mobile telecommunication technology. Firstly, the first generation (1G) is an analog system capable of voice communication. The second generation (2G) was introduced in the late 1990s and it was known as the global system for mobile communication (GSM) its main advantage was the use of a digital system. The third generation (3G) was the beginning of mobile broadband telecommunication, where data communication was the main focus and led to the rapid growth of data services, such as internet, media, voice over IP (VoIP), etc. The fourth generation (4G) or long-term evolution (LTE) results from the development of the 3G technology. It implemented the carrier aggregation and multiple input multiple output (MIMO) techniques to enhance the frequency bandwidth, the data throughput, and the latency. Nowadays, the fifth generation (5G) is published to enhance mobile broadband, ultra-reliable and low-latency communication. The application of 5G can be observed in various fields, such as in the media and entertainment field, the machines are communicated in the manufacturing process, and telemedicine is one main priority, autonomous vehicles or self-driving cars, surveillance as discussed in [1–4]

As a result, the antenna is one of the important parts of 5G technology, especially the base station antenna needs to improve for compact size, high gain, uni-directional radiation pattern, and multiple frequency bands [5]. There are numerous studies on the design and development of the base station antenna as follows: The use of the metamaterial structure as the means to enhance the efficiency of the antenna [6–8], The drawbacks are only that the metamaterial is very small in size, therefore the fabrication would be challenging. Superstrate and electromagnetic band gap (EBG) are another technique to reduce the mutual coupling and enhance the gain, by placing the dielectric material in front of the antenna [9–11], which would eventually lead to the new technique called partially reflective surface (PRS), using the dielectric with the microstrip patch to act as the reflective element to further enhance the gain of the antenna [11],[12]. Array antenna is one of the techniques to increase the gain of the antenna. Having the same element placed in order repeatedly, meaning the characteristics of each element are relevant to other elements, results in enhancement of the characteristics of the antenna. However, this enhancement would lead to cross-polarization, coupling by the element nearby. As can be seen in [13–14]. Therefore, designing the antenna as the array is challenging and daring.

The dual-band S-patch antenna with gain enhancement by using the planar array configuration and dielectric superstrate is introduced in this paper. It is the base station antenna based on the 5G frequency bands n41 (2.6 GHz) and n78 (3.5 GHz). The S-patch antenna is a single element and arranged in the 2 × 6 elements planar array antenna and the FR4 dielectric superstrate is on the top of the array. The simulated results indicated

that the operating frequency of 2.5–2.6 GHz and 3.4–3.6 GHz with uni-directional radiation pattern. The rest of this paper is in section 2 antenna structure, simulated and measured results are discussed in sections 3 and 4, and the conclusion is in section 5.

2. Dual-Band S-Patch Antenna Structure

The S-patch antenna is introduced to a single element of a planar array antenna, which consists of a radiation patch, dielectric substrate, and ground plane as shown in **Figure 1**. The FR4 is employed as the substrate with ε_r equal to 4.3 and thickness = 3.2 mm. The radiation patch is the S character with the probe feed at the top right corner of the S patch as shown in **Figure 1**.

Based on the antenna structure illustrated in **Figure 1**, simulations were conducted utilizing the CST microwave studio [15]. Upon modifying the antenna parameters as specified in **Table 1**, the results indicated that it can be operated in two frequency bands. Due to the meander line of S, it can be resonant with two frequency bands of 2.55–2.65 GHz and 3.46–3.61 GHz with a unidirectional radiation pattern. **Figure 2** shows that the $|S_{11}|$ less than -10 dB at 2.55–2.65 GHz and 3.46–3.61 GHz and the radiation pattern at 2.6 GHz and 3.5 GHz are shown in **Figures 3–4** with a gain of 3.98 dBi at 2.6 GHz and 4.1 dBi at 3.5 GHz. It is noted that the cross-polarization of the proposed antenna is lower than -10 dB at 2.6 GHz and 3.5 GHz. The design of the single element with the dimensions of the proposed antenna is shown in **Figure 1** and **Table 1**, respectively. Initially, the microstrip patch antenna is introduced with the FR4 as the main material of the substrate. The ground plane is located at the back of the microstrip patch.

To adjust the frequency response, the slits and slots are added to the patch, resulting in the "S-Shaped" patch [16].

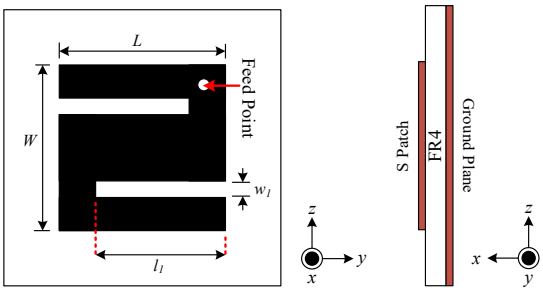

Figure 1 The geometry of dual-band S-patch antenna.

Table 1 Parameter of the dual-band S-patch antenna.

Parameters	Physical Size (mm)
L	43.00
W	43.00
l_1	38.00
w_1	2.00

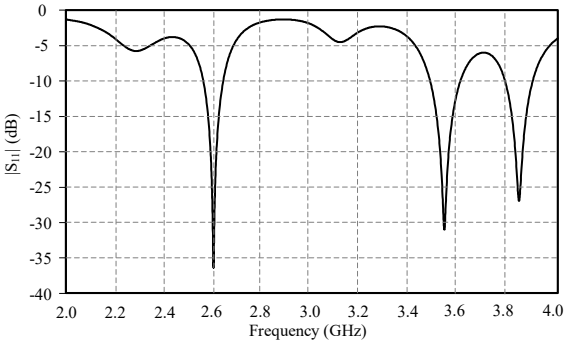

Figure 2 Simulated $|S_{11}|$ of the dual-band S-patch antenna.

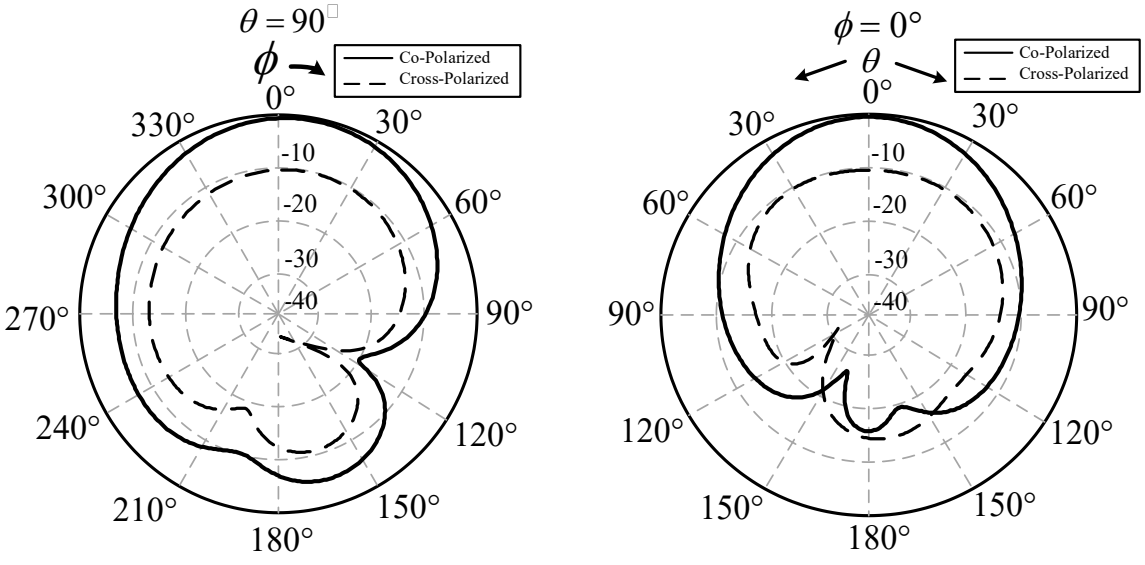

Figure 3 Simulated the radiation pattern at 2.6 GHz. (**a**) *xy* plane (**b**) *xz* plane.

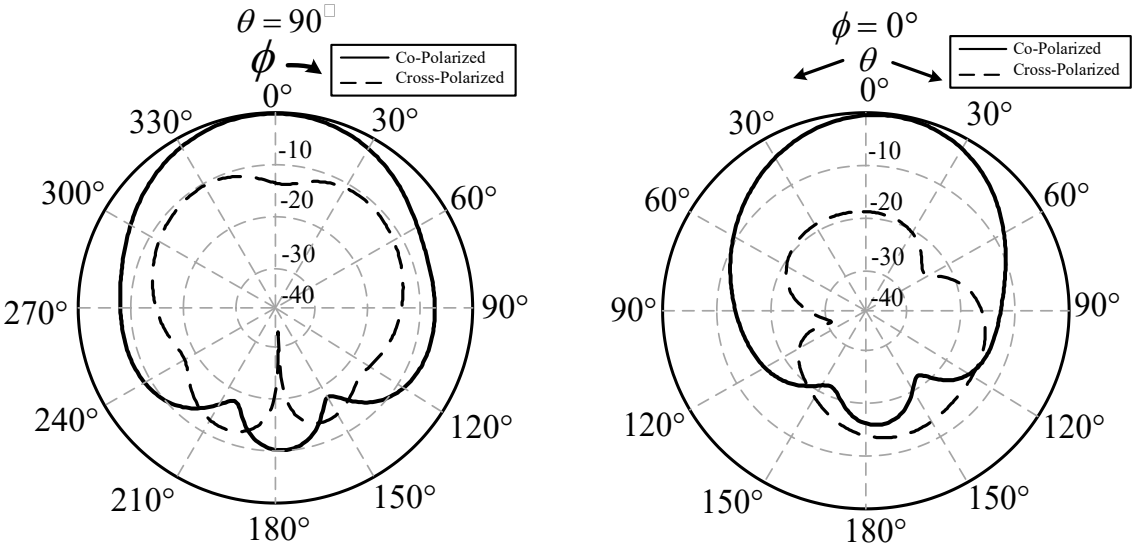

Figure 4 Simulated the radiation pattern at 3.5 GHz. (**a**) xy plane (**b**) xz plane.

3. Dual-Band S-Patch Antenna Array

From Section 2, the dual-band S-patch antenna is introduced. The planar array configuration and dielectric superstrate are proposed in this section by using the array element of the S-patch antenna. Antenna array formation is the arrangement of multiple antenna elements to control the direction and shape of the radiation pattern by the principle of pattern multiplication. By adjusting the number of elements, array form, spacing, phase, and amplitude of signals, the antenna can focus energy in desired directions, reduce interference, and improve gain. The S-patch antenna is then rearranged in a planar array configuration by using 2 × 6 elements with a distance of each element of 87 mm and the dielectric superstrate of FR4 with a thickness of 3.2 mm is put in front of the array antenna in the distance (*D*) of 15 mm as shown in **Figure 5**. Since the structure is meant to be mounted on the base station tower, this layout is used to restrict its width, then the total size of the antenna array is 132 mm in width and 450 mm in length.

Based on ray propagation theory, adjusting the cavity height that the dielectric superstrate from the antenna contributes to improvements in both gain and directivity. Eq. (1) provides an estimation of the antenna's maximum directivity coefficient [17].

$$D = \frac{c}{4\pi f} + (\varphi_{PRS} + \varphi_{GND} - 2N\pi) \qquad (1)$$

where *D* is the gap of the cavity; *N* is the order of the resonance mode (i.e., *N* = 0, 1, 2,…); *f* is the resonance frequency; *c* is the speed of light in free space; φ_{PRS} is the reflection phase of the superstrate; and φ_{GND} is the reflection phase of the ground plane. Utilizing an FR4 dielectric superstrate with a thickness of 3.2 mm, positioned at a distance of 15 mm (*D*) from the antenna element, has been shown to enhance both gain and directivity.

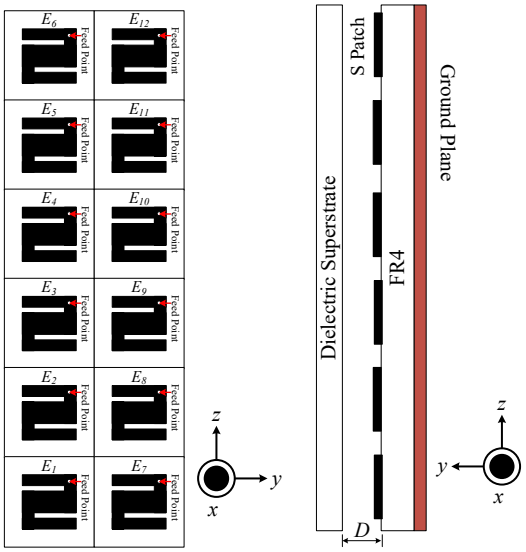

Figure 5 The geometry of dual-band S-patch antenna array of 2 × 6 elements.

The characteristics of the array antenna are then analyzed, where the currents of each element are set to be equal but the effect of coupling between the elements [18], which occurs when more than two antennas are placed close together, is taken into account. The $|S_{mm}|$ of each element is investigated as shown in **Figure 6** where m = 1, 2, …., 12. Since the antenna array structure is symmetrical, only the results of elements 1 to 6 are displayed. From the results, it was found that the $|S_{mm}|$ value still resonates at two frequency bands, 2.55–2.65 GHz and 3.46–3.61 GHz, but it can be seen that the $|S_{mm}|$ value of each component has a slight shift, which is a result of the coupling between the array elements.

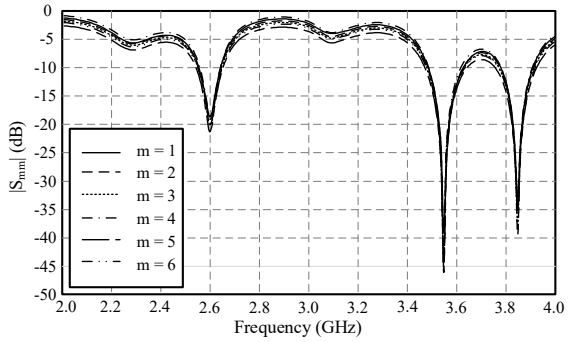

Figure 6 Simulated $|S_{mm}|$ of dual-band S-patch antenna array of 2 × 6 elements.

Next, the isolation coefficient is considered to determine the coupling behavior of the array element between the elements arranged along the *z*-axis, where only elements 1 to 6 are considered here due to the symmetrical antenna construction. The $|S_{mn}|$ of each element is investigated as shown in **Figure 7** where m and n = 1, 2, …., 12. In **Figure 7**, it can be seen that the $|S_{mn}|$ values of all elements are less than -20 dB throughout the frequency range, which indicates that each element has a low coupling signal and can work separately efficiently. Note that $|S_{mn}|$ levels are strongest when the elements are close together, such as m = 1 n = 2, m = 2 n = 3, m = 3 n = 4, m = 4 n = 5 and m = 5 n = 6, etc. Then there will be a decrease in intensity level depending on the distance between the elements such as m = 1 and n = 3, 4, 5, and 6, etc.

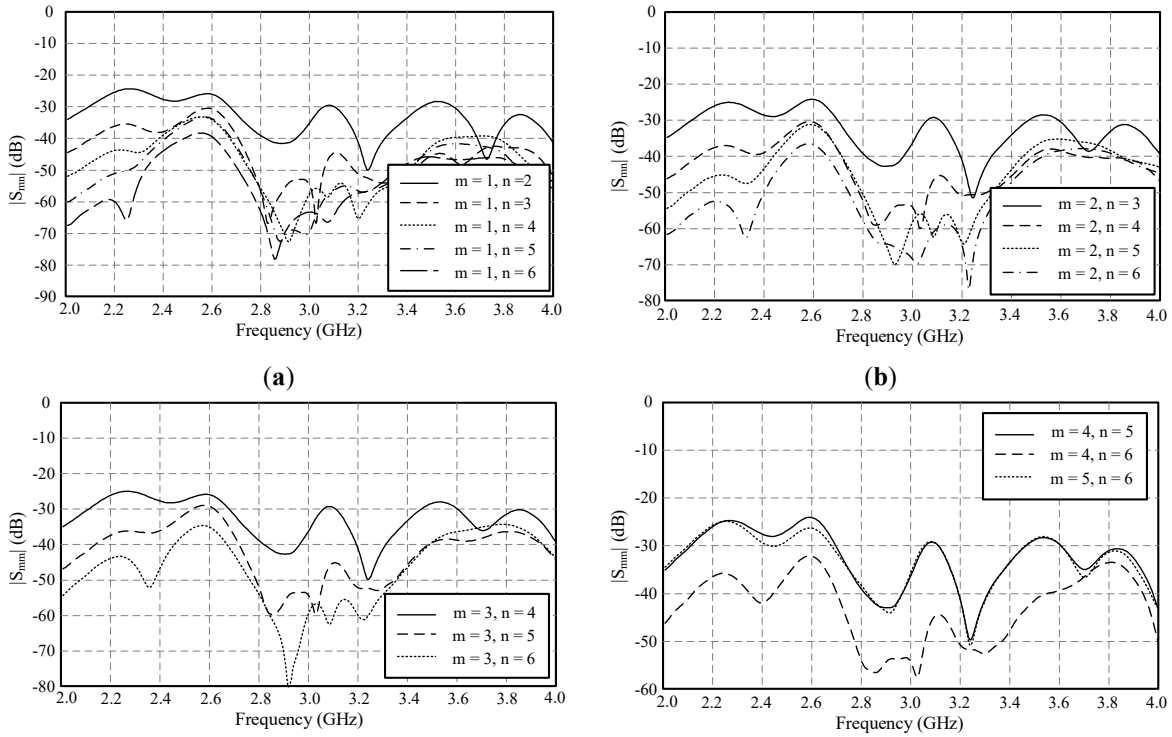

Figure 7 Simulated $|S_{mn}|$ of dual-band S-patch antenna array of 2 × 6 elements along the *z*-axis. (**a**) $|S_{1n}|$ (**b**) $|S_{2n}|$ (**c**) $|S_{3n}|$ and (**d**) $|S_{4n}|$ and $|S_{5n}|$.

In addition, the isolation coefficient between each element along the *y*-axis was considered as shown in **Figure 8**. It was found that the $|S_{mn}|$ values of all elements are less than -20 dB throughout the frequency range. Note that $|S_{mn}|$ levels are strongest when the elements are close together, such as m = 1 n = 7, m = 2 n = 8, and m = 3 n = 9 etc. Then there will be a decrease in intensity level depending on the distance between the elements such as m = 1 n = 8, 9, 10, 11 and 12, etc.

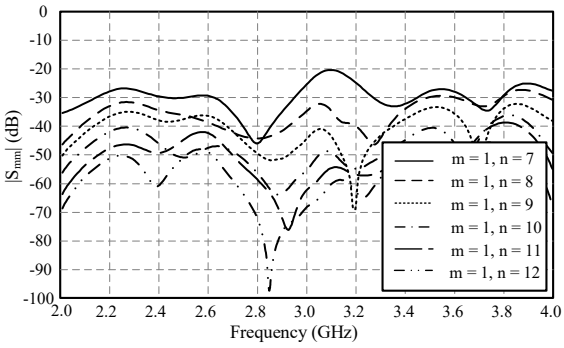

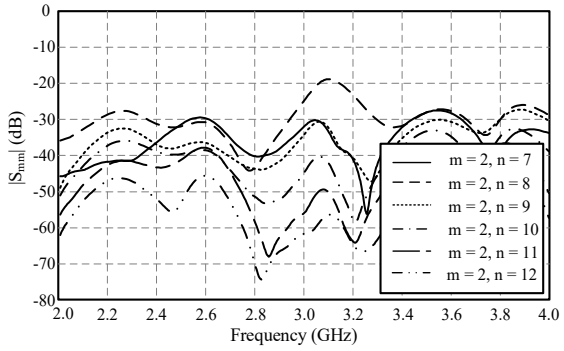

(**b**)

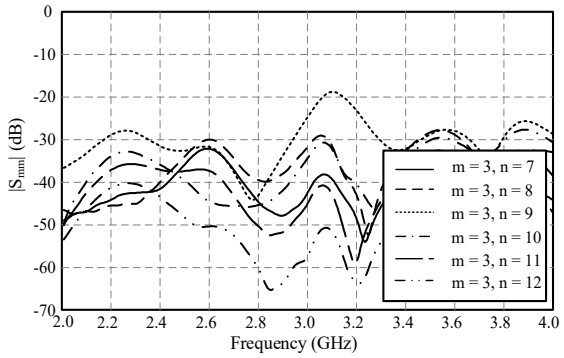

(**c**)

Figure 8 Simulated $|S_{mn}|$ of dual-band S-patch antenna array of 2 × 6 elements along the *y*-axis. (**a**) $|S_{1n}|$ (**b**) $|S_{2n}|$ and (**c**) $|S_{3n}|$.

There are notable variations when the 2 × 6 element antenna array is taken into account because of the radiating elements' constructive and destructive interference effects. The pattern multiplication principle can be used to discuss it [18]. The array factor (AF) for a 2 × 6 element planar array antenna with uniform amplitude and spacing can be employed as follows Eq. (2):

$$AF(\theta,\phi)=\sum_{m=1}^{M} I_m e^{j(m-1)(kd_x \sin\theta\cos\phi+\beta_x)} \sum_{n=1}^{N} I_n e^{j(n-1)(kd_y \sin\theta\cos\phi+\beta_y)} \quad (2)$$

where M and N are the numbers of elements, I_m and I_n are the amplitude of the element along the *x*- and *y*-axis, β_x and β_y are the phase of the element along the *x*- and *y*-axis, and d_x and d_y are the distance between elements of the array. The planar array geometry is shown in **Figure 9.**

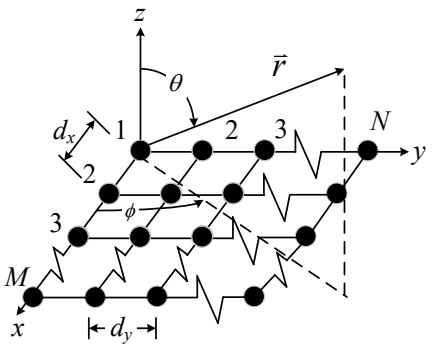

Figure 9 The planar array geometries.

From the simulated results in **Figures 10–11**, antenna arrays can produce much narrower beams by combining the radiation of multiple elements with specific phase and amplitude settings. It has significant side lobes of -8.00 dB and -9.00 dB at 2.6 GHz and 3.5 GHz, respectively due to the interference between radiating elements. The side lobes are undesirable in applications like communication systems because they can cause interference or loss of energy. However, it achieves a much higher gain 16.07 dBi and 15.90 dBi at 2.6 GHz and 3.5 GHz, respectively. The gain of an array increases with the number of elements, as the radiated power is concentrated in a narrower beam. It is noted that the cross-polarization of the proposed antenna is lower than -10 dB at 2.6 GHz and 3.5 GHz. Furthermore, as **Table 2** illustrates, the FR4 superstrate can increase the antenna array gain in two frequency bands while maintaining a high antenna efficiency. However, there are efficiencies of less than 60% and the primary sources of efficiency degradation in the proposed antennas include dielectric and conductor losses, and surface wave generation, all of which contribute to reduced radiated power and overall efficiency.

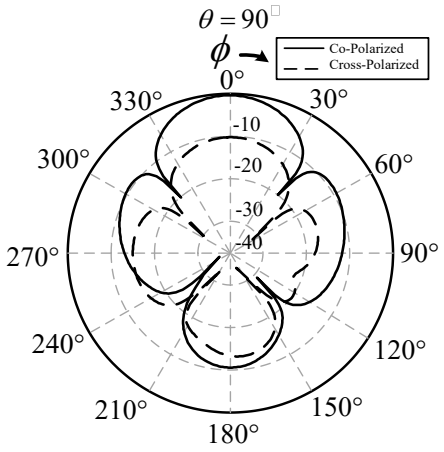

(**a**) *xy* plane.

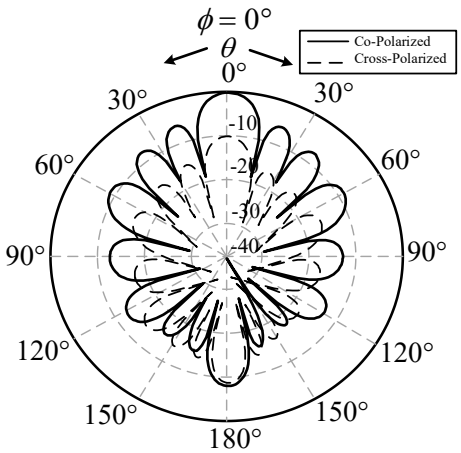

(**b**) *xz* plane.

Figure 10 Simulated the radiation pattern of dual-band S-patch antenna array of 2 × 6 elements at 2.6 GHz.

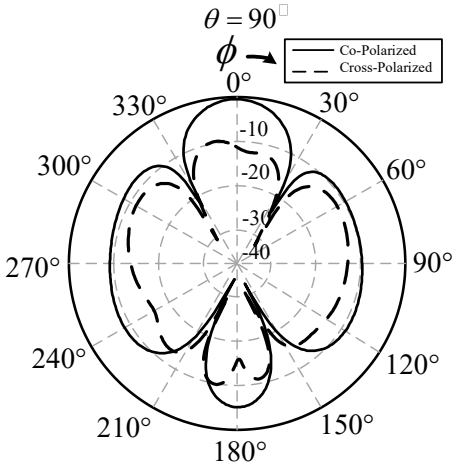

(**a**) *xy* plane.

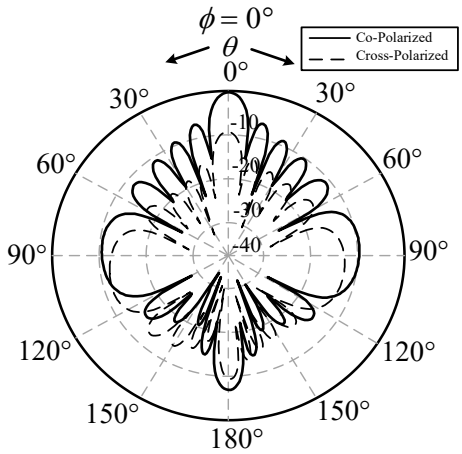

(**b**) *xz* plane.

Figure 11 Simulated the radiation pattern of dual-band S-patch antenna array of 2 × 6 elements at 3.5 GHz.

Table 2 Comparison of gain and efficiency dual-band S-patch antenna array of 2 × 6 elements at 2.6 GHz and 3.5 GHz with and without superstrate.

Antenna Array	Gain (dBi)		Efficiency (%)	
	2.6 GHz	3.5 GHz	2.6 GHz	3.5 GHz
With Superstrate	16.07	15.9	53.77	49.78
Without Superstrate	15.14	15.49	45.58	42.79

4. Measurement

Based on the simulation results presented in the previous section, a prototype antenna was fabricated using a substrate of FR4 material with a thickness of 3.2 mm. The dielectric superstrate is fabricated from FR4 material with a thickness of 3.2 mm. **Figure 12** illustrates the prototype of the dual-band S-patch antenna array consisting of 2 × 6 elements operating. After that, The antenna is fed to each element with equal signal amplitude and phase using a 1:16 Wilkinson power divider. The prototype antenna was carried out in an anechoic chamber using the vector network analyzer (VNA) (Keysight FieldFox Series) to obtain accurate S-parameters and radiation patterns across the target frequency range. A standard horn antenna served as a reference for gain comparison, with all measurements conducted under far-field conditions. The S-parameters of the prototype antenna are analyzed to evaluate the impedance matching and isolation coefficient. The $|S_{mm}|$ of each element is investigated as shown in **Figure 13** where m = 1, 2, …., 12. Since the antenna array structure is symmetrical, only the results of elements 1 to 6 are displayed. From the results, it was found that the $|S_{mm}|$ value still resonates at two frequency bands, 2.55–2.65 GHz and 3.46-3.61 GHz, but it can be seen that the $|S_{mm}|$ value of each component has a slight shift, which is a result of the coupling between the array elements.

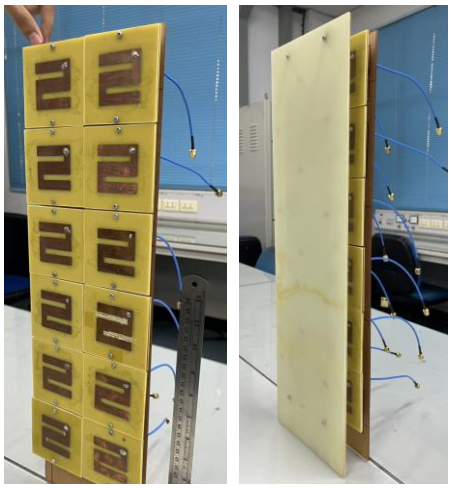

Figure 12 Prototype of dual-band S-patch antenna array of 2 × 6 elements.

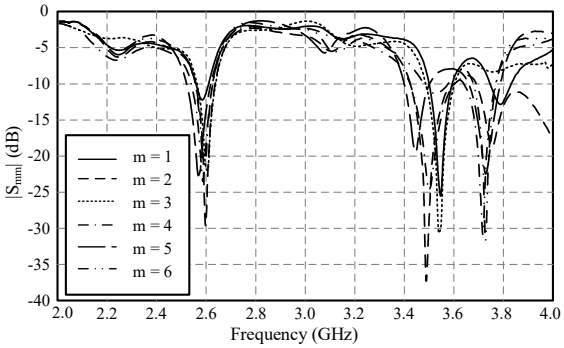

Figure 13 Measured $|S_{mm}|$ of dual-band S-patch antenna array of 2 × 6 elements.

Next, the isolation coefficient is considered to determine the coupling behavior of the array element between the elements arranged along the *z*-axis, where only elements 1 to 6 are considered here due to the symmetrical antenna construction. The $|S_{mn}|$ of each element is investigated as shown in **Figure 14** where m and n = 1, 2, …., 12. In **Figure 14**, it can be seen that the $|S_{mn}|$ values of all elements are less than -20 dB throughout the frequency range, which indicates that each element has a low coupling signal and can work separately efficiently. Note that $|S_{mn}|$ levels are

strongest when the elements are close together, such as m = 1 n = 2, m = 2 n = 3, m = 3 n = 4, m = 4 n = 5, and m = 5 n = 6, etc. Then there will be a decrease in intensity level depending on the distance between the elements such as m = 1 n = 3, 4, 5 and 6, etc.

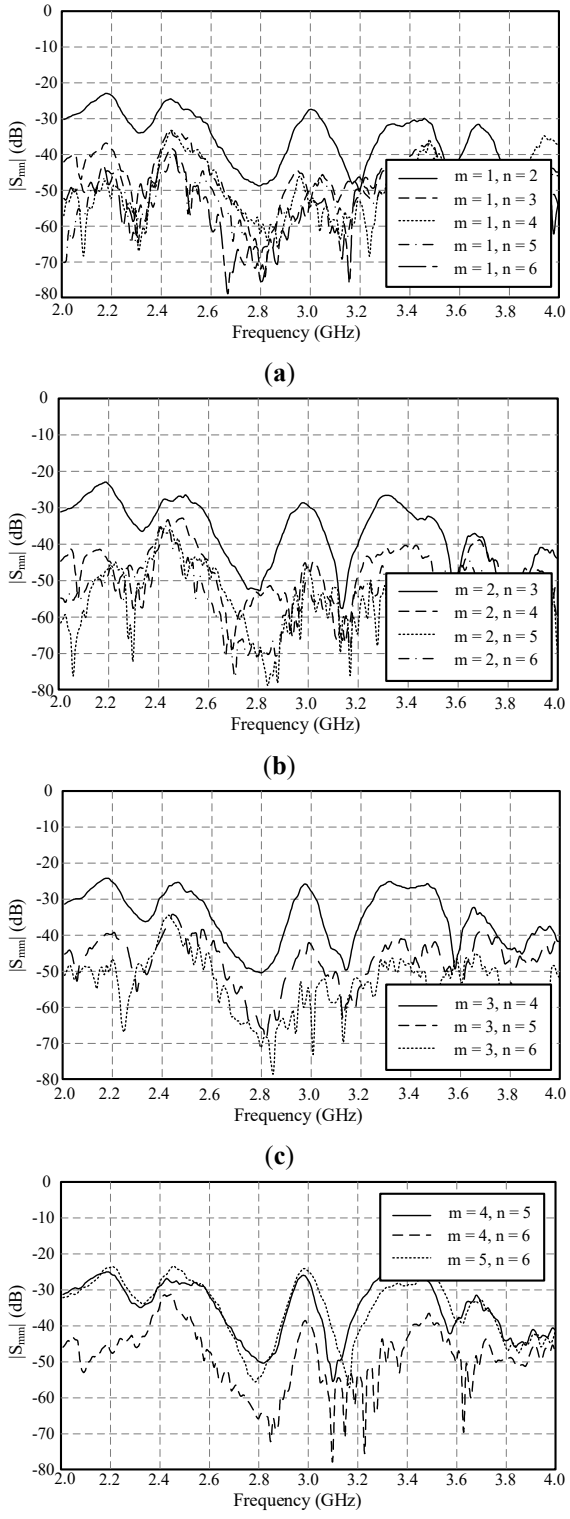

Figure 14 Measured $|S_{mn}|$ of dual-band S-patch antenna array of 2 × 6 elements along the *z*-axis.

In addition, the isolation coefficient between each element along the *y*-axis was considered as shown in **Figure 15**. It was found that the $|S_{mn}|$ values of all elements are less than -20 dB throughout the frequency range. Note that $|S_{mn}|$ levels are strongest when the elements are close together, such as m = 1 n = 7, m = 2 n = 8, and m = 3 n = 9, etc. Then there will be a decrease in intensity level depending on the distance between the elements such as m = 1 n = 8, 9, 10, 11 and 12, etc.

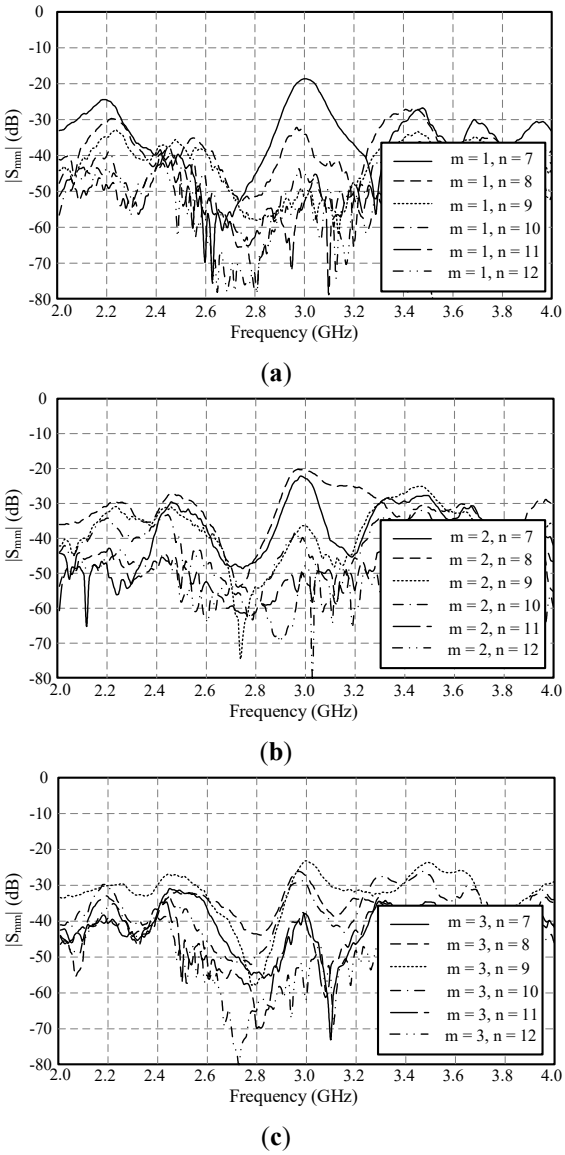

Figure 15 Measured $|S_{mn}|$ of dual-band S-patch antenna array of 2 × 6 elements along the *y*-axis.

From the measured results in **Figures 16–17**, antenna arrays can produce much narrower beams by combining the radiation of multiple elements with specific phase and amplitude settings. It has significant side lobes of -9.00 dB and -10.00 dB at 2.6 GHz and 3.5 GHz, respectively due to the interference between radiating elements. The side lobes are undesirable in applications like communication systems because they can cause interference or loss of energy. However, it achieves a

much higher gain 18.70 dBi and 19.30 dBi at 2.6 GHz and 3.5 GHz, respectively. The gain of an array increases with the number of elements, as the radiated power is concentrated in a narrower beam. It is noted that the cross-polarization of the proposed antenna is lower than -10 dB at 2.6 GHz and 3.5 GHz. In addition, a comparison of the antenna gain, half-power beamwidth (HPBW), and side lobe level (SLL) between the simulated and measured results is conducted at the operating frequency as shown in **Table 3**.

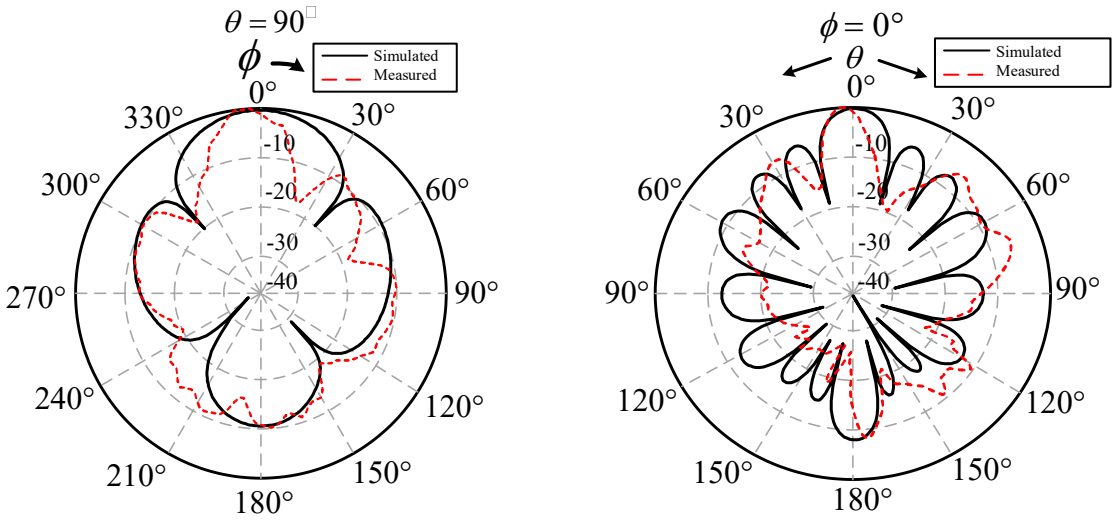

(**a**) *xy* plane. (**b**) *xz* plane.

Figure 16 The radiation pattern of dual-band S-patch antenna array of 2 × 6 elements at 2.6 GHz.

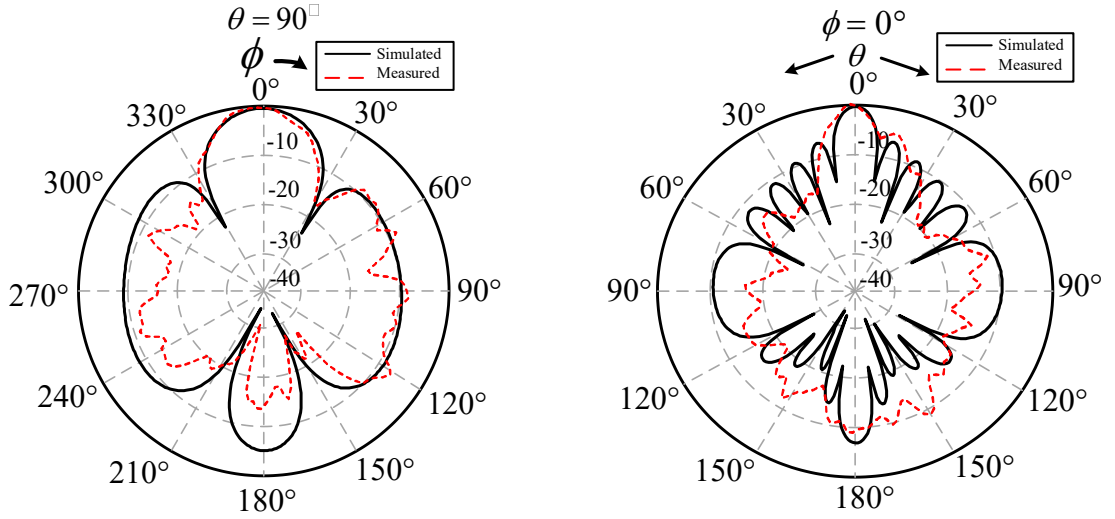

(**a**) *xy* plane. (**b**) *xz* plane.

Figure 17 The radiation pattern of dual-band S-patch antenna array of 2 × 6 elements at 3.5 GHz.

Table 3 Antenna gain, HPBW and SLL of dual-band S-patch antenna array of 2 × 6 elements at 2.6 GHz and 3.5 GHz.

Results	**Gain (dBi)**		**HPBW (degree)**		**SLL (dB)**	
	2.6 GHz	3.5 GHz	2.6 GHz	3.5 GHz	2.6 GHz	3.5 GHz
Simulated	16.07	15.9	16.0	16.5	-8.0	-9.0
Measured	18.70	19.30	14.0	15.0	-9.0	-10.0

It should be noted that discrepancies between the measured and simulated results are primarily attributed to mutual coupling effects among the antenna elements, nuts, poles, and mounting structures. Nevertheless, the results remain acceptable within the context of laboratory-scale experiments. To ensure suitability for real-world 5G base station applications, the prototype antenna must be housed within a radome and affixed to a stable structural mounting point.

5. Conclusion

The dual-band S-patch antenna is designed and fabricated for 5 G base stations operating in the n41 (2.6 GHz) and n78 (3.5 GHz) frequency bands. A 2 × 6 planar array configuration is utilized with an FR4 dielectric superstrate, the antenna achieves an

enhanced gain of 18.70 dBi at 2.6 GHz and 19.30 dBi at 3.5 GHz, with a uni-directional radiation pattern. Simulated and measured results demonstrate good agreement, confirming the antenna's performance and suitability for base station applications due to its simple design.

6. References

[1] A. A. Ahmed Solyman and K. Yahya, "Evolution of wireless communication networks: from 1G to 6G and future perspective," *International Journal of Electrical and Computer Engineering (IJECE)*, vol. 12, no. 4, pp. 3943–3950, 2022, doi: 10.11591/ijece.v12i4.pp3943-3950.

[2] A. Gohar and G. Nencioni, "The Role of 5G Technologies in a Smart City: The Case for Intelligent Transportation System," *Sustainability*, vol. 13, no. 9, 2021, Art. no. 5188, doi: 10.3390/su13095188.

[3] M. Javaid, A. Haleem, R. P. Singh, R. Suman, "5G technology for healthcare: Features, serviceable pillars, and applications," *Intelligent Pharmacy*, vol. 1, no. 1, pp. 2–10, 2023, doi: 10.1016/j.ipha.2023.04.001.

[4] G. Gkagkas, D. J. Vergados and A. Michalas, "The advantage of the 5G network for enhancing the Internet of Things," in 2021 6th South-East Europe Design Automation, Computer Engineering, Computer Networks and Social Media Conference (SEEDA-CECNSM), Preveza, Greece, Sep. 24–26, 2021, pp. 1–7, doi: 10.1109/SEEDA-CECNSM53056.2021.9566239.

[5] M. Farasat, D. N. Thalakotuna, Z. Hu, Y. Yang, "A Review on 5G Sub-6 GHz Base Station Antenna Design Challenges," *Electronics*, vol. 10, no. 16, 2021, Art. no. 2000, doi: 10.3390/electronics10162000.

[6] X. Shi, Y. Cao, Y. Hu, X. Luo, H. Yang and L. H. Ye, "A High-gain Antipodal Vivaldi Antenna With Director and Metamaterial at 1–28 GHz," *IEEE Antennas and Wireless Propagation Letters*, vol. 20, no. 12, pp. 2432–2436, 2021, doi: 10.1109/LAWP.2021.3114061.

[7] Y. Dong and T. Itoh, "Metamaterial-Based Antennas," *Proceedings of the IEEE*, vol. 100, no. 7, pp. 2271–2285, 2012, doi: 10.1109/JPROC.2012.2187631.

[8] N. Hussain, M. -J. Jeong, A. Abbas, T. -J. Kim and N. Kim, "A Metasurface-Based Low-Profile Wideband Circularly Polarized Patch Antenna for 5G Millimeter-Wave Systems," *IEEE Access*, vol. 8, pp. 22127–22135, 2020, doi: 10.1109/ACCESS.2020.2969964.

[9] F. Yang and Y. Rahmat-Samii, "Microstrip antennas integrated with electromagnetic band-gap (EBG) structures: a low mutual coupling design for array applications," *IEEE Transactions on Antennas and Propagation*, vol. 51, no. 10, pp. 2936–2946, 2003, doi: 10.1109/TAP.2003.817983.

[10] A. K. Singh, M. P. Abegaonkar and S. K. Koul, "High-Gain and High-Aperture-Efficiency Cavity Resonator Antenna Using Metamaterial Superstrate," *IEEE Antennas and Wireless Propagation Letters*, vol. 16, pp. 2388–2391, 2017, doi: 10.1109/LAWP.2017.2719864.

[11] M. Ahirwar and V. Singh Chaudhary, "Enhancing Antenna Performance: Exploring Partially Reflective Surfaces as Superstrates," in *2024 IEEE International Students' Conference on Electrical, Electronics and Computer Science (SCEECS)*, Bhopal, India, 2024, pp. 1–4, doi: 10.1109/SCEECS61402.2024.10482245.

[12] N. Santalunai, S. Santalunai, W. Naktong, P. Chaipanya, P. Mesawad and P. Krachodnok, "Advancements in Mobile Communication: A Novel Sectoral Antenna Design Incorporating Magneto-Electric Curved Strip Dipoles and PRS Superstrate," *IEEE Access*, vol. 12, pp. 29837–29849, 2024, doi: 10.1109/ACCESS.2024.3369489.

[13] Z. Wang, G. -x. Zhang, Y. Yin and J. Wu, "Design of a Dual-Band High-Gain Antenna Array for WLAN and WiMAX Base Station," *IEEE Antennas and Wireless Propagation Letters*, vol. 13, pp. 1721–1724, 2014, doi: 10.1109/LAWP.2014.2352618.

[14] G. Singh, G. Singh, A. Kumar, B. C. Sahoo and D. Singh, "Design and Analysis of Slotted Antenna Array for Vehicular Applications," in *2024 11th International Conference on Signal Processing and Integrated Networks (SPIN)*, Noida, India, Mar. 21–22, 2024, pp. 134–138, doi: 10.1109/SPIN60856.2024.10511090.

[15] Dassault Systèmes. "Electromagnetic Simulation Solvers: CST Studio Suite Simulation Solvers for Electromagnetic Systems and Devices" 3ds.com. https://www.3ds.com/products/simulia/cst-studio-suite/electromagnetic-simulation-solvers (accessed Jan. 1, 2025).

[16] S. K. Patel and Y. P. Kosta, "S-Shape meandered microstrip patch antenna design using metamaterial," in *2014 IEEE Antennas and Propagation Society International Symposium (APSURSI)*, Memphis, TN, USA, 2014, pp. 547–548, doi: 10.1109/APS.2014.6904604.

[17] X. Sheng, X. Lu, N. Liu and Y. Liu, "Design of Broadband High-Gain Fabry–Pérot Antenna Using Frequency-Selective Surface," *Sensors*, vol. 22, no. 24, 2022, Art. no. 9698, doi: 10.3390/s22249698.

[18] C. A. Balanis, "Arrays: Linear, Planar, and Circular," in *Antenna Theory Analysis and Design*, 4 th. ed., New York, NY, USA: John Wiley & Sons, Inc., 2005, ch. 6, sec. 6.10, pp. 348–360.